



AFRL-RX-WP-TP-2011-4208

**THE ROLE OF MICROTTEXTURE ON THE FATIGUE
BEHAVIOR OF AN $\alpha + \beta$ TITANIUM ALLOY, Ti-6Al-2Sn-
4Zr-6Mo (PREPRINT)**

J.M. Larsen

Metals, Ceramics, and NDE Division

C.J. Szczepanski and S.K. Jha

Universal Technology Corporation

J.W. Jones

University of Michigan

MARCH 2011

Approved for public release; distribution unlimited.

See additional restrictions described on inside pages

STINFO COPY

**AIR FORCE RESEARCH LABORATORY
MATERIALS AND MANUFACTURING DIRECTORATE
WRIGHT-PATTERSON AIR FORCE BASE, OH 45433-7750
AIR FORCE MATERIEL COMMAND
UNITED STATES AIR FORCE**

REPORT DOCUMENTATION PAGE

Form Approved
OMB No. 0704-0188

The public reporting burden for this collection of information is estimated to average 1 hour per response, including the time for reviewing instructions, searching existing data sources, gathering and maintaining the data needed, and completing and reviewing the collection of information. Send comments regarding this burden estimate or any other aspect of this collection of information, including suggestions for reducing this burden, to Department of Defense, Washington Headquarters Services, Directorate for Information Operations and Reports (0704-0188), 1215 Jefferson Davis Highway, Suite 1204, Arlington, VA 22202-4302. Respondents should be aware that notwithstanding any other provision of law, no person shall be subject to any penalty for failing to comply with a collection of information if it does not display a currently valid OMB control number. **PLEASE DO NOT RETURN YOUR FORM TO THE ABOVE ADDRESS.**

1. REPORT DATE (DD-MM-YY) March 2011		2. REPORT TYPE Journal Article Preprint		3. DATES COVERED (From - To) 01 March 2011 – 01 March 2011	
4. TITLE AND SUBTITLE THE ROLE OF MICROTTEXTURE ON THE FATIGUE BEHAVIOR OF AN $\alpha + \beta$ TITANIUM ALLOY, Ti-6Al-2Sn-4Zr-6Mo (PREPRINT)				5a. CONTRACT NUMBER In-house	
				5b. GRANT NUMBER	
				5c. PROGRAM ELEMENT NUMBER 62102F	
6. AUTHOR(S) J.M. Larsen (AFRL/RXLM) C.J. Szczepanski and S.K. Jha (Universal Technology Corporation) J.W. Jones (University of Michigan)				5d. PROJECT NUMBER 4347	
				5e. TASK NUMBER 20	
				5f. WORK UNIT NUMBER LM121100	
7. PERFORMING ORGANIZATION NAME(S) AND ADDRESS(ES) Metals, Ceramics, and NDE Division (AFRL/RX) Air Force Research Laboratory Materials and Manufacturing Directorate Wright-Patterson Air Force Base, OH 45433-7750 Air Force Materiel Command, United States Air Force				8. PERFORMING ORGANIZATION REPORT NUMBER AFRL-RX-WP-TP-2011-4208	
Universal Technology Corporation Dayton, OH 45432					
University of Michigan Materials Science and Engineering Ann Arbor, MI 48109					
9. SPONSORING/MONITORING AGENCY NAME(S) AND ADDRESS(ES) Air Force Research Laboratory Materials and Manufacturing Directorate Wright-Patterson Air Force Base, OH 45433-7750 Air Force Materiel Command United States Air Force				10. SPONSORING/MONITORING AGENCY ACRONYM(S) AFRL/RXLM	
				11. SPONSORING/MONITORING AGENCY REPORT NUMBER(S) AFRL-RX-WP-TP-2011-4208	
12. DISTRIBUTION/AVAILABILITY STATEMENT Approved for public release; distribution unlimited.					
13. SUPPLEMENTARY NOTES PAO Case Number: 88ABW 2010-5845; Clearance Date: 02 Nov 2010. Document contains color. Journal article submitted to <i>Acta Materialia</i> .					
14. ABSTRACT The effect of microstructural heterogeneity, specifically regions of grains with similar crystallographic orientations, or microtexture, on the initiation and early growth of fatigue cracks from multiple micro-notches has been investigated in Ti-6246. Experiments were performed using ultrasonic fatigue techniques for two different microstructural conditions. Local texture surrounding micro-notches was found to influence micro-notch fatigue crack initiation in one of the microstructures. Fatigue crack initiation was least likely to occur from notches placed in neighborhoods with a microtexture unfavorably oriented for easy basal slip. However, small fatigue crack propagation rates were not influenced by the microtexture in these local neighborhoods. A systematic variation in micro-notch length indicated that fatigue cracks initiated from naturally occurring microstructural features when micro-notches with a surface length (2c) less than 15-20 μm were machined in specimens.					
15. SUBJECT TERMS microtexture, $\alpha + \beta$ titanium alloys, small fatigue crack growth, fatigue crack initiation					
16. SECURITY CLASSIFICATION OF:			17. LIMITATION OF ABSTRACT: SAR	18. NUMBER OF PAGES 48	19a. NAME OF RESPONSIBLE PERSON (Monitor) Andrew Rosenberger 19b. TELEPHONE NUMBER (Include Area Code) N/A
a. REPORT Unclassified	b. ABSTRACT Unclassified	c. THIS PAGE Unclassified			

The Role of Microtexture on the Fatigue Behavior of an $\alpha + \beta$ Titanium Alloy,
Ti-6Al-2Sn-4Zr-6Mo

C. J. Szczepanski¹; S. K. Jha¹; J. M. Larsen; and J. W. Jones²

Air Force Research Laboratory, Materials and Manufacturing Directorate, AFRL/RX, Wright-Patterson Air Force Base, OH 45433 USA

¹Universal Technology Corporation, Dayton, OH 45432 USA

²University of Michigan, Materials Science and Engineering, Ann Arbor, MI 48109 USA

Keywords: microtexture, $\alpha + \beta$ titanium alloys, small fatigue crack growth, fatigue crack initiation

Abstract

The effect of microstructural heterogeneity, specifically regions of grains with similar crystallographic orientations, or microtexture, on the initiation and early growth of fatigue cracks from multiple micro-notches has been investigated in Ti-6246. Experiments were performed using ultrasonic fatigue techniques for two different microstructural conditions. Local texture surrounding micro-notches was found to influence micro-notch fatigue crack initiation in one of the microstructures. Fatigue crack initiation was least likely to occur from notches placed in neighborhoods with a microtexture unfavorably oriented for easy basal slip. However, small fatigue crack propagation rates were not influenced by the microtexture in these local neighborhoods. A systematic variation in micro-notch length indicated that fatigue cracks initiated from naturally occurring microstructural features when micro-notches with a surface length ($2c$) less than 15-20 μm were machined in specimens. Fatigue crack growth rates of short and long fatigue cracks were used to predict fatigue lifetimes, which agreed with experimentally observed worst-case fatigue lifetimes from smooth-bar fatigue tests conducted at 20 kHz. The predicted scatter in fatigue lifetimes resulting from experimentally observed variability in small fatigue crack growth only accounted for 0.1% of the total observed fatigue lifetime variability.

Since scatter in lifetimes is essentially eliminated for specimens with a starting artificial defect size ($2c$) of approximately $20\ \mu\text{m}$, it is concluded that the variability in fatigue lifetime results from the inherent variability in the microstructurally controlled process of initiating small fatigue cracks approximately $20\ \mu\text{m}$ in size.

1. Introduction

In a previous study[1], we examined the role of microstructure on the crack initiation behavior of a microtextured $\alpha + \beta$ Ti-6246 alloy in the very high cycle fatigue (VHCF) regime under loading conditions where nominally elastic behavior is expected ($\sigma_{\text{max}} = 0.4\text{-}0.6\ \sigma_{\text{YS}}$ [$\sigma_{\text{YS}} \equiv$ yield stress]). This work was motivated by an interest in determining if microstructure variability, and its effect on fatigue crack initiation, could explain the substantial variability that was observed for fatigue lives in the range of 10^6 to 10^9 cycles. Fractography revealed that crack initiation and/or early propagation produced a higher than average number of basal plane facets resulting from slip deformation. However, the only defining characteristic associated with individual initiation sites was that the α -phase material surrounding the initiation sites was favorably textured to support basal or prismatic slip, which has been shown to result from the prior β texture.[2] No clear distinctions could be drawn to classify local microstructures leading to short or long fatigue lifetimes. Therefore, it was of interest to quantify the variability in fatigue lives resulting from microstructurally-dependent differences in the very early stages of crack propagation. This can be described as an extension of Hall's phenomenological model for titanium alloys as:

$$N_f = N_i(M_1) + N_s(M_2) + N_\sigma(M_3) + N_\delta(M_4)$$

where N_i , N_s , N_σ , and N_δ are the numbers of cycles required for initiation, small crack growth, long crack growth, and final fracture, respectively.[3] M_1 - M_4 represent the fact that microstructure may

have different effects on each of the individual stages of the fatigue process. For example, microstructural neighborhoods that exhibit high fatigue crack initiation resistance (e.g. regions of small grains) will not necessarily exhibit high resistance to long fatigue crack growth processes. It is anticipated that very little of the scatter results from long fatigue crack growth. However, it is expected that processes sensitive to local microstructure, i.e. fatigue crack initiation and small fatigue crack growth, will contribute most significantly to the variability observed in fatigue lifetimes. In the present paper we extend our previous research by investigating the role of microstructure and, in particular, microtexture on the fatigue crack growth behavior of Ti-6246. The objective of the current work is to determine the role of microstructural heterogeneity on variability in fatigue lifetime through its small and long fatigue crack growth contributions. Previous studies indicate that local microstructural heterogeneity can significantly influence fatigue behavior, and these studies are reviewed in the remainder of this section.

It is well known that nominal microstructural characteristics, such as average grain size or macroscopic texture, strongly correlate with mean fatigue behavior of structural alloys.[4,5,6] However, the short-life extreme in a fatigue lifetime distribution is of primary interest in the design and life management practices for fracture critical components.[7,8] Jha and coworkers [9] have demonstrated that the life-limiting failures can be predicted by assuming that fatigue crack initiation occurs immediately and that minimum specimen lifetimes are determined by the combined small and long fatigue crack propagation behavior. Others have analyzed the characteristics of anomalous microstructural features leading to fatigue crack initiation and early growth and postulated potential mechanisms by which agglomerates of similarly oriented grains may affect fatigue behavior.[10-22] However, the link between microstructural heterogeneity

and the variability in total fatigue lifetime is not as well understood. Only a few studies [15,16] have examined the influence of microstructural heterogeneity on the distribution in fatigue lifetimes for structural alloys.

Reports in the literature suggest that crack growth behavior in titanium alloys is affected by texture. The anisotropy in mechanical properties of titanium alloys has led to numerous investigations of the role of texture on the fatigue behavior of this class of alloys.[5,6,17,18] Some researchers have related the role of microstructure on fatigue properties to testing environment,[17] while others have ascribed it to the accommodation of plasticity at the crack tip resulting from local microstructural configurations.[18] Bowen investigated the impact of strong textures on the fatigue crack growth properties of Ti-6Al-4V.[18] He observed that crystals oriented for prism slip exhibited the highest fatigue crack growth rates. Specifically, if deformation is symmetric about the crack tip, slow fatigue crack growth is expected. However, if only one slip system is activated, and asymmetric deformation was observed, then the fatigue crack growth rates were measurably higher. Peters and coworkers investigated the role of texture on mechanical properties in Ti-6Al-4V having a fine, equiaxed microstructure.[17] For testing in vacuum, they observed increased fatigue crack growth resistance for specimens with a texture in which most of the grains were oriented with their basal poles perpendicular to the loading axis. The high fatigue crack growth resistance of these planes was diminished for testing in air and 3.5 percent NaCl solutions. Thus, the benefit of loading along this crystallographic direction was eliminated due to the detrimental role of environment.

In recent years, other researchers have addressed the role of microtexture on the observed fatigue behavior of alpha + beta titanium alloys.[11-14,19,20] Sinha et al. established that microtextured regions are the critical fatigue crack initiation sites under dwell fatigue conditions at high stresses ($\sigma/\sigma_{YS}=0.95$) and that the size of the microtextured region ultimately determined which location was responsible for initiating the life-limiting fatigue crack.[11] They speculated that it was easier for a small fatigue crack to propagate through a microtextured region where all the grains have nominally similar crystallographic orientations, but that the potential for crack arrest exists at the edge of microtextured regions where crack deflection may be necessary to continue propagation along preferred crystallographic planes. Thus, large microtextured regions were more likely to produce larger fatigue cracks than small microtextured regions, and these large cracks would have higher stress intensity factors, thereby increasing the likelihood that these cracks would lead to specimen failure. LeBiavant et al. observed that multiple fatigue cracks initiated in grains favorably oriented for slip within each microtextured region and that the fatal fatigue crack formed as a result of the linkup of the individual cracks.[12] Both of these studies highlighted the effect that microtextured regions may have on fatigue crack growth behavior.

There are limited reports in the literature regarding the role of microtexture on fatigue crack growth rates although in recent years there are more reports detailing the significance of local microstructure on small fatigue crack growth behavior. The work of Zhai, et al. indicates that the twist between the active slip planes in adjacent grains determines the small fatigue crack growth rates.[21,22] As a fatigue crack approaches a grain boundary, if a large deflection from the crack path is required, a deceleration of the crack, and potentially crack arrest, may be observed. At grain boundaries where cracks did not need to deflect, it was observed that the

growth rates were not affected by the grain boundary. Recent work by Marx and coworkers agrees with this concept and they state that cracks decelerate as they approach grain boundaries if there is a large misorientation between the active slip planes in both grains.[23] This observation agrees with an earlier investigation of fatigue crack initiation and early growth by Krupp and co-workers in a β -titanium alloy. Interestingly, they observed that slip incompatibility between adjacent grains leads to fatigue crack initiation, but that microstructural regions with small misorientations between adjacent grains were found to be favorable for small crack growth.[24] Based on their observations in Ti-Mn alloys, Saleh and Margolin point out that the existence of the Burgers orientation relationship does not enable easy slip transfer across α/β phase boundaries and that these boundaries can significantly affect growth rates.[25]

If one considers the plastic zone for small fatigue cracks, it is reasonable to think that adjacent grains with similar crystallographic orientations are likely to enhance small fatigue crack growth rates, or in other words, the grain boundaries in these regions are unlikely to pose significant obstacles to small fatigue crack propagation. To illustrate this logic, one may envision three distinct categories of microstructural neighborhoods: (a) a microtextured region in which the grains are favorably oriented for slip, (b) a randomly textured region, and (c) a microtextured region unfavorably oriented for slip. In a general sense, these characteristic microstructural neighborhoods will generate fatigue crack growth rates representing the full spectrum of fatigue behavior for a given microstructure. It is easy to imagine that small crack propagation rates would be higher in a microtextured region when an advancing fatigue crack encounters many grains that are favorably oriented for slip (a), as compared to a microstructural neighborhood in which the majority of grains are unfavorably oriented for slip leading to crack retardation and

arrest at grain boundaries (c). Within this phenomenological construct, it would be expected that a microstructural neighborhood with random texture (b) would exhibit growth rates similar to those observed within an unfavorably oriented microtextured region due to the necessity of propagating cracks across high angle grain boundaries and phase interfaces. This simplified model to describe the role of microstructure on small fatigue crack growth is analogous to the slip accumulation mechanism reported for fatigue crack initiation and early growth processes in various materials.[10,11,21,23,24] The orientation of a few grains are likely to have a more pronounced effect on small fatigue crack growth rates than they would in the regime of long fatigue crack growth, where the crack tip is interacting with many more grains and the propagation rates are expected to converge to an average value. Thus, characterization of small fatigue crack growth behavior in specific microtextured neighborhoods is a necessary step in quantifying the inherent variability in fatigue behavior resulting from microstructural heterogeneity.

2. Experimental Procedure

The material used in this study, Ti-6Al-2Sn-4Zr-6Mo, was processed to produce an $\alpha + \beta$ microstructure. For the purpose of investigating the role of microtexture on fatigue damage propagation properties, micro-notches were machined in samples from two different microstructures; one containing microtexture (microstructure A) and the other with a random texture (microstructure B). Representative backscattered electron (BSE) micrographs and the β phase inverse pole figure (IPF) maps for the two microstructures investigated are shown in Figure 1. Samples from microstructure A were extracted from a forged pancake, while samples from microstructure B were extracted from a part that had undergone more complex forging

operations similar to those used in industrial manufacturing processes. For microstructure A, shown in Figure 1(a) and (c), the nominal primary α (α_p) grain size was $3.7 \pm 2.4 \mu\text{m}$, as measured by the linear intercept method, and the volume fraction of α_p grains was approximately 27%. In microstructure B, Figure 1(b) and (d), the α_p grain size was $4.6 \pm 2.3 \mu\text{m}$ and the volume fraction of α_p grains was 38%. Thus, the overall microstructural morphology is considered to be similar for these two materials. IPF maps show that the prior β grain size was typically on the order of 20-40 μm in microstructure A, while for microstructure B, it was 10-30 μm . However, clusters of similarly oriented prior β grains as large as a few hundred micrometers are commonly observed in microstructure A, but not in microstructure B.[2] The crystallographic orientation of the secondary (lath) α phase is inherited upon transformation from the β phase. The α_p grain orientations are expected to be independent of the secondary α texture due to the dynamic spheroidization process that controls α_p formation.[26] Although, local regions may exhibit similar α_p and secondary α textures due to localization of deformation in the $\alpha + \beta$ phase field forming operations.[27]

Ultrasonic fatigue tests in the current study were completed at $R=0.05$, 20 kHz, room temperature in laboratory air, and stresses (σ_{max}) ranging from 500-600 MPa, which replicated conditions used for S-N tests previously reported.[1] Cylindrical ultrasonic fatigue specimens with a reduced gage section of 4 mm were used in this study. To facilitate observation of fatigue crack growth from micro-notches, two diametrically opposed flats were machined in the specimen gage to produce flat regions extending the entire 12 mm gage length and covering 2 mm in width. All specimens were electropolished in a solution of 590 ml methanol, 350 ml butyl cellosolve, and 60 ml perchloric acid at -40°C and 40 V to remove compressive residual

stresses that result from machining. Approximately 100 μm of material was removed from the specimen surface, which exceeds the depth of compressive residual stresses according to reported residual stress depth profiles for low stress grinding.[28]

In the course of this experimental effort, various approaches were used to assess the validity of using ultrasonic fatigue techniques to investigate microstructurally sensitive fatigue crack growth. To compare ultrasonic frequency fatigue crack growth rates with conventional frequency data, single micro-notches, nominally 100 μm in length (2c) were introduced at the center of the flats by femtosecond laser (FSL) machining in five specimens. The FSL machining technique has been shown to be essentially free of damage at the notch tip.[29-31] Fatigue crack growth rates for cracks emanating from these notches during ultrasonic fatigue serve as a comparison with long fatigue crack growth behavior under conventional testing conditions.

To determine the length scale at which local microstructure affects small fatigue crack growth rates, a focused ion beam (FIB) microscope was used to machine micro-notches in fatigue specimens. A range of microstructural neighborhoods were probed in individual specimens by machining 5 micro-notches in each flat for a total of 10 micro-notches in each specimen, as shown schematically in Figure 2. In this set of 13 specimens, the FIB micro-notches were spaced approximately 2-3 mm apart. Notches were randomly placed in the above manner to investigate both the role of notch size on cycles to initiation and to examine small fatigue crack growth behavior. A Nova NanoLab FIB microscope with a gallium ion source operating at 30 kV and a probe current of 6.5 nA was employed to machine micro-notches with a height of approximately 3 μm and surface lengths ranging from 14-37 μm , and in all cases $c/a=1$. Collateral damage has

been reported to be insignificant (i.e. $< \sim 1 \mu\text{m}$ thick), and machining conditions were selected to minimize collateral damage, while maintaining reasonable machining rates.[32] The use of multiple FIB notches in each fatigue specimen enabled more small fatigue crack data to be acquired with fewer specimens, and to examine the variability in growth rates as a function of differences in microstructure in the notch neighborhood.

In one specimen for each microstructure, notches were placed to maximize differences in local microtexture to examine the role of microtexture on small crack growth. Local texture in a $200 \times 200 \mu\text{m}$ region at these locations was determined by electron backscattered diffraction (EBSD) at a resolution of $0.5 \mu\text{m}$. Within these regions, a second localized EBSD scan ($65 \times 90 \mu\text{m}$) at a higher resolution of $0.2 \mu\text{m}$ was performed to enable identification of specific α_p grains and α laths for subsequent analysis of crystallographic influences on the crack path. Figures 3 and 4 display representative neighborhoods that were characterized in the localized EBSD scans with notch location indicated schematically on each IPF map. Figures 5 and 6 illustrate the same microstructural information surrounding the notches examined in microstructure B. Shown in the first column are α phase IPF maps, the second column displays β phase IPF maps, and the IPFs corresponding to the α phase are shown in the third column. The loading axis is vertical, and the colors in the IPF maps correspond to the [001] direction, which is the loading axis. The more concentrated nature of the texture intensity peaks in the IPFs for microstructure A (Figures 3 and 4) as compared with those in microstructure B (Figures 5 and 6) substantiate that the local texture is sharper in microstructure A. The colors in the IPF maps correspond to the key in Figure 7, which illustrates the (a) α phase orientations, (b) β phase orientations, and (c) the locus of maximum Schmid factors (≥ 0.475) for each of the individual slip systems. In titanium alloys,

basal and prism slip are the most commonly observed deformation mechanisms at room temperature, while pyramidal slip is commonly observed to be a hard slip mode.[33] Since the microstructural feature of interest was the local texture, which is related to the prior β grain orientation, it was assumed that scans of the specimen surface were representative of the local material texture just below the surface as well. Notch locations were selected based on consideration of both the α and β phase textures.

To begin each test, blocks of approximately 5,000-10,000 cycles were applied, and acetate replicas were made after every cycle block to inspect each notch for fatigue crack initiation. The quality of the replicas permitted identification of crack extension on the order of a few (3-5) micrometers. Once a fatigue crack had initiated from one of the micro-notches, cycle intervals were decreased to approximately 2,000-3,000 cycles between replication steps. This was held constant so that sample-interval induced error would not be a factor in comparing crack growth data from different specimens. It should be noted that the use of multiple micro-notches in each specimen avoids this problem, since all notches inherently experience the same cycle intervals for a given sample. The stress intensity factor range (ΔK) was calculated using the stress intensity solutions of Newman and Raju [34] for a surface crack in a finite elastic plate and c/a is assumed to be 1. ΔK values presented here were calculated for the crack tip at the maximum crack depth ($\phi=\pi/2$). The thickness of the specimen used was the distance between the flats which was typically about 3 mm. The crack growth rate data were processed using SMOOTH, which averages out experimental measurement error over the full range of crack measurements.[28]

3. Results and Discussion

The simplified description of microstructure presented in the Introduction does not account for local variations in microstructural morphology, such as variability in α_p grain size, α lath size, volume fraction of α , which would all be expected to affect local mechanical properties including small fatigue crack behavior. Chan and Lankford suggested that “small” cracks become “short” once the crack intersects approximately 20 grains.[35] If one considers the average α_p grain size of approximately 4 μm , this criterion for microstructural similitude would be achieved for a crack with a depth (a) of 25 μm . Thus, even the smallest notches produced via FIB would satisfy the similitude criterion in the early stages of small crack growth. However, if the critical crack growth controlling microstructural feature is defined as the prior β grain size, which is on the order of 20 μm , then similitude would only be achieved once the crack depth (a) was approximately 125 μm . Therefore, as a first cut, the fatigue crack growth results are interpreted as an effect of microtexture since the impact of any particular α lath or α_p grain is presumed to be statistically insignificant once the similitude criterion is achieved ($a \geq 25 \mu\text{m}$) for these smaller features.

In the remainder of this paper the term “small” crack is used to describe cracks initiating from FIB micro-notches, and which are presumed to initially experience a state of microstructural dissimilitude as opposed to “short” cracks, which are defined as being still physically small, but have achieved the microstructural similitude criterion.[36] The role of microtexture on fatigue crack growth behavior is expected to be manifested in the small crack regime. Thus, small crack behavior will be presented in the analysis of microstructural effects on crack growth, while long fatigue crack growth data are used for comparison with other frequencies and in the prediction of

lifetimes. Fatigue behavior of small and long cracks is addressed separately in the following sections.

3.1 Long Fatigue Crack Growth Behavior

The crack growth rate data acquired at 20 kHz in the long crack regime ($\Delta K > 5 \text{ MPa}\cdot\text{m}^{1/2}$) from laser machined micro-notches are presented in Figure 8. The growth rates observed in cracks initiating from laser-machined notches at ultrasonic frequencies are shown in open symbols.[37] The red curve in this plot represents a prediction of the long crack growth rates in the same material (microstructure A) at a stress ratio of $R=0.05$ based on crack growth rates measured from fatigue testing over a range of stress ratios in C(T) specimens.[27,38] Fatigue crack growth data measured at conventional frequencies (20 Hz) from naturally initiated cracks are shown by the solid symbols for comparison.[7] Fatigue crack growth rates agree in each of these techniques and validate that ultrasonic frequency testing yields fatigue crack growth data that are similar to the growth rates measured with conventional techniques. Additionally, there is a negligible stress level effect across the stress levels investigated, i.e. 500-600 and 860 MPa. The agreement in growth rates across frequencies and testing conditions engendered confidence in the applicability of ultrasonic frequency fatigue techniques to the characterization of fatigue crack growth behavior. There was little variability observed in these growth rates, which led to an increased focus on smaller crack lengths where the impact of local microstructural variability is expected to be more significant.

3.2 Small Fatigue Crack Growth Behavior

3.2.1 Effect of notch size

In each individual sample, 10 micro-notches of equal dimensions were machined using the FIB. FIB micro-notch lengths ($2c$) ranged from 14-37 μm , but all notches had a height of approximately 3 μm , and an appropriate depth so that $c/a=1$. Various notch sizes were examined in different specimens in this study and Figure 9 illustrates the fraction of notches that initiated in each specimen as a function of notch size. As the figure shows, in specimens with a notch size ($2c$) of 37 μm , all notches were observed to initiate fatigue cracks. In the case of 14-15 μm FIB micro-notches, a few notches initiated small cracks, but fatal fatigue cracks were never observed to initiate from notches of this size. A specimen with 20 μm notches was tested from microstructure A, but cracks did not initiate from these notches. However, when 23-25 μm notches were machined in samples of microstructure A, crack initiation was typically observed from 50%-80% of the notches. In microstructure B, 50% of notches with a surface length ($2c$) on the order of 18-19 μm typically initiated. The critical notch size where 50% of notches were observed to initiate fatigue cracks is of interest, because micro-notches of this size provide insight into the role of microstructural neighborhoods in promoting or inhibiting natural fatigue crack initiation and growth.

While crack initiation occurred for a few notches with a dimension $2c = 15 \mu\text{m}$, these cracks did not propagate beyond one grain diameter, as shown in Figure 10(a). In fact, specimens with 10 randomly placed 15 μm FIB notches failed from subsurface fatigue crack initiation, as shown in the fractograph in Figure 10(b). The major axis diameter of this facet at the fatigue crack initiation site was approximately 15 μm , which was equivalent to the micro-notch size. The observation of subsurface fatigue crack initiation suggested that this specific microstructural neighborhood accumulated plasticity much more easily than the microstructural region near the

FIB notch. This is especially true when one considers the lack of constraint at the specimen surface and the substantially higher stress intensities at the notch tips relative to the initially undeformed microstructure. The lifetime to failure for this specimen was 2.94×10^8 cycles. Using previously published data to predict lifetimes, a lifetime of approximately 10^6 cycles would be expected if the crack had initiated in the first cycle.[37] This implies that a substantial portion of the lifetime was consumed by the fatigue crack initiation process. For the case of a notch this size, the calculated stress intensity factor range at the notch tips was approximately $2 \text{ MPa}\cdot\text{m}^{1/2}$. This is below the conventional long crack growth fatigue threshold ($\Delta K_{th} \sim 3 \text{ MPa}\cdot\text{m}^{1/2}$).[27] However, in this material at these loading conditions, a known small fatigue crack effect has been observed, with cracks propagating under a ΔK of $2 \text{ MPa}\cdot\text{m}^{1/2}$. [7] While it is not entirely accurate to compare micro-notch initiated cracks to naturally initiated cracks, the fact that FIB notches with a surface length of approximately $20 \text{ }\mu\text{m}$ lead to crack initiation would suggest that the controlling microstructural dimension is on this length scale. Furthermore, this length scale corresponds to the typical fatigue crack initiation size observed in surface initiated fatigue cracks in typical round bar S-N fatigue tests.[1,15] Individual α_p facets observed at surface initiated failure sites were on the order of $5 \text{ }\mu\text{m}$, but generally a cluster of multiple facets extending over a distance of $15\text{-}20 \text{ }\mu\text{m}$ composed the crack initiation and early growth region.

3.2.2 *Fatigue crack growth rates*

All small fatigue crack growth data collected from specimens with FIB notches are shown in Figure 11 for microstructure A and microstructure B. The aforementioned prediction (c.f. Figure 8) of long crack growth rates (solid line) is also shown in this plot for comparison.[27] The average fatigue crack growth rates in microstructure B are somewhat lower than in

microstructure A. This observation supports the phenomenological model described earlier. Specifically, the extremes of hypothetical microstructural conditions (i.e. microtextured regions favorably (a) and unfavorably (c) oriented for slip) that encompass the full range of fatigue crack growth behavior would be expected to occur in microstructure A, therefore producing higher average growth rate. However, since microstructure B has a more random texture, it would be expected that fewer adjacent grains are favorably oriented for easy fatigue crack extension across grain boundaries. This hypothesis is in agreement with the observation of lower average fatigue crack growth rates in microstructure B.

Figures 12(a) and (b) present the $2c$ vs. N and the fatigue crack growth rates, respectively, in microstructure A, while Figures 12(c) and (d) similarly illustrate the fatigue crack propagation behavior in microstructure B. In both of the $2c$ vs. N plots, periods of crack acceleration, deceleration, and arrest were observed for various cracks. It is apparent from a comparison of Figures 12(a) and (c) that once a crack began propagating in microstructure A, it generally continued to propagate, whereas in microstructure B, crack retardation and arrest was more prevalent. This may be a result of the difference in microstructure, where small cracks in microstructure A typically encounter only a few prior β grains due to the larger prior β grain (and α colony) size, while a crack of a similar size propagating through microstructure B would typically traverse many more grain and phase boundaries. This could lead to crack retardation or arrest as the crack approached the prior β grain boundaries and needed to re-initiate within each new prior β grain. The slower fatigue crack growth rates observed in microstructure B can also be explained by considering the global difference in volume fraction of α_p grains between microstructure A and B. α_p grains are generally not expected to have similar crystallographic

orientations as adjacent α laths. Thus, crack path deflection at both α_p and prior β grain boundaries may be required for microstructure B more often than for microstructure A. Such behavior is in agreement with reports from Sinha and coworkers, in which crack arrest was observed as fatigue cracks propagated to the edge of a microtextured region favorably oriented for basal and prismatic slip.[11] Their observation is notable in establishing the effect of microtexture on fatigue crack propagation, since they worked at considerably higher stresses ($0.9-0.95 \sigma_{YS}$) where crack arrest would seem to be less likely.

From the plots in Figure 12(b) and (d), it is clear that both microstructures exhibit a small crack effect relative to long fatigue crack growth data. Variability in fatigue crack growth rates is observed in the small crack regime, but significantly less as cracks continued to propagate, which is expected as metallurgical similitude is achieved.[35,36] Fatigue crack growth rates for the small cracks generally converge to the long crack behavior at a stress intensity factor of approximately $5 \text{ MPa}\cdot\text{m}^{1/2}$. At the stress level investigated ($\sigma_{\max}=600\text{MPa}$), a stress intensity range of $5 \text{ MPa}\cdot\text{m}^{1/2}$ corresponds to a crack depth (a) of approximately $60 \mu\text{m}$. This value falls between the values where microstructural similitude is achieved if one considers either α_p grains or prior β grains as the fatigue critical microstructural features. This result indicates that the interaction of small fatigue cracks with local microstructure is a complex process and cannot simply be ascribed to the characteristics of a single constituent phase.[35]

3.2.3 *Local texture surrounding micro-notches*

The local textures surrounding these micro-notches have been investigated and no dependence of growth rates on texture was observed. While textures suitable for basal and prism slip did lead to

earlier fatigue crack initiation in microstructure A, no correlation between local texture and initiation lifetime or propagation rates was observed in microstructure B. The IPF maps of the investigated microstructural neighborhoods for the specimen from microstructure A are presented in ranked order of increasing fatigue crack initiation lifetime in Figures 3 and 4. The α phase IPF maps are labeled in the lower left-hand corner with the crack IDs which correspond to the crack growth data shown in Figure 12(a) and (b). This information is also summarized in Table I, which relates crack IDs to initiation lifetime and relative growth rates for the specimen from microstructure A. Relative fatigue crack growth rates were determined by examining the small fatigue crack regime of the da/dN vs. ΔK plots in Figure 12(b) and (d). When the earliest cracks to initiate were considered in the aggregate, notches placed in regions where the β phase material was favorably oriented for $\{110\}$ slip led to earlier fatigue crack initiation. The schematic IPF in Figure 7(c) depicts the locus of Schmid factor maxima ($SF \geq 0.475$) for the easily activated basal and prism slip systems as well as the harder first order pyramidal $\langle a \rangle$ -type slip system, which is useful for interpreting the textures depicted with the IPFs. Using this as a guide to classify the local textures, it is clear that the earliest cracks to initiate in microstructure A, namely A7, A8, and A6, all have a texture intensity peak near the maximum Schmid factor for basal slip and in one case (A8) a texture intensity peak favorably oriented for prism slip is observed, as well. Similarly, Figures 5 and 6 display IPF maps for regions surrounding the notches in microstructure B for the first four and the subsequent four notches to initiate fatigue cracks, respectively. These figures also correspond to the crack IDs shown in Figure 12(c) and (d). This information is summarized in Table II, which again relates the crack ID with initiation lifetime and relative growth rate. Comparison of the IPFs in Figures 5 and 6 indicates that there is no correlation between texture type and small fatigue crack growth rates for microstructure B.

The lack of correlation in texture and growth rates can be explained in microstructure B due to the weak local texture and the fact that the prior β grains were smaller than the micro-notches. Thus, it was not always possible to machine a notch within one prior β grain, which made it difficult to experimentally isolate the effects of specific prior β grain orientations. However, even for microstructure A, individual fatigue crack growth rates did not correlate with local texture. This observation highlights the fact that relating fatigue crack growth rates to microstructure may require a more quantitative description of microtextured regions and local microstructural morphology. These quantitative descriptions of microstructure are possible via three dimensional characterization techniques such as tomography and post-mortem serial sectioning. Additionally, the lack of correlation in local texture and growth rates indicates that these microtextured regions may not be severe enough to measurably influence small fatigue crack growth rates.

Another analysis of these data is shown on the plot in Figure 13(a) and (b) for microstructures A and B, respectively. These semi-quantitative plots relate observed texture (intensity and character) to the crack growth rates relative to other cracks in the same specimen. Since the local texture is a continuously varying property, only general classifications (i.e. basal/prism, pyramidal) were used to describe texture. The local textures were classified using the IPFs in Figures 3-6 as a general guide. Local texture (character and intensity) did not correlate with the fatigue crack growth rates measured from these notches. Coupling these results with the fatigue crack path observations suggests that the microtextured regions in this alloy are not textured strongly enough to significantly affect crack growth rates. In other words, despite the

microtexture, there are enough grains (α_p and lath α) with different orientations and interfaces throughout the microstructure that can perturb growth rates.

3.2.4 Crack path observations

BSE micrographs of the fastest and slowest propagating cracks in microstructure A are shown in Figure 14(a) and (b), respectively. The horizontal lines on the micrographs indicate the length of the crack as measured in each replica and the vertical ticks within the micrograph indicate the position of the crack tip within the microstructure for a given cycle count. The numbers above each line indicate the cycle count and crack length (in micrometers) when the replica was made.

Crack A6, as shown in Figure 14(a), took slightly longer to initiate, but it should be noted that once it initiated, it grew at a faster rate than crack A8, displayed in Figure 14(b) (c.f. Table I, Figure 12a and 12b). For example, between 21,340 cycles and 44,780 cycles, crack A8 grew approximately 40 μm , while in the same period crack A6 initiated and propagated approximately 100 μm . Since these cracks were subjected to the same external loads, this variability in growth rates can be attributed to the microstructure ahead of the crack tip. The difference likely arises because of crack deflection at an α_p grain boundary in the slower growing crack. An additional example of the influence of microstructure on growth rates is observed by comparing the left and right sides of crack A8. Between 28,030 and 44,780 cycles the crack shown in Figure 14(b) propagated only 10 μm on the left side, while it extended 22 μm on the right side in the same cycle interval. For both cracks, replicas often revealed that an α_p grain boundary was coincident with the crack tip. It is plausible that some of these cases are random occurrences, since replicas provide snapshots of crack length, as opposed to continuous monitoring of crack extension.

However, in light of the apparent crack arrest and subsequent crack path deviations away from α_p grains, it is clear that the α_p grain boundaries and the grain orientations influence fatigue crack growth rates. The decreased growth rates due to the interaction of cracks with α_p grains is not surprising considering that on average α_p grains are not expected to maintain similar crystallographic orientations as the adjacent lath α , because of the dynamic spheroidization process by which the grains form.[26]

The corresponding Schmid factor (SF) intensity maps are shown in Figure 15, where separate colors denote the individual quintiles of Schmid factors as illustrated in the legend. The notch shape and crack path have been extracted from BSE micrographs and are overlaid in white on these SF intensity maps. Figures 15(a) and (b) are the Schmid factor plots for basal and prism slip in the fastest propagating crack from microstructure A (crack A6, Figure 14a), and Figure 15(c) and (d) display the same data from the same microstructure for the crack with the slowest propagation rate (crack A8, Figure 14b). The SF maps indicate that the material immediately adjacent to notch A8 is more favorably oriented for basal slip as compared to notch A6, which is consistent with the observation of earlier fatigue crack initiation from notch A8. Despite this favorable orientation for basal slip, however, crack A8 propagates more slowly than crack A6. A number of factors could contribute to this observation: the material in the specimen interior is unfavorably oriented for slip, or the microstructural morphology may be affecting growth rates. It is reasonable to assume that these microtextured regions extend a few hundred micrometers below the surface.[2] Thus, this observation points to the fact that interfaces within the microstructure, such as grain and phase boundaries, provide a barrier to small fatigue crack extension, even in cases where adjacent features may be favorably oriented for easy deformation.

3.3 Lifetime predictions

Using the experimentally observed variability in fatigue crack growth rates to establish the bounds of small fatigue crack growth behavior, predictions of the range in expected fatigue lifetimes can be made, assuming that a fatigue crack initiates in the first fatigue cycle. These predictions are shown on the S-N curve in Figure 16, and it is clear that the worst case (surface initiated) failures are accurately captured by these predictions. The bounding lines for worst-case fatigue lifetimes were generated using separate power law fits to experimental data for both the small and long fatigue crack growth rates. Predictions of the small fatigue crack growth contribution to total lifetime were made by integrating the Paris law from a starting crack size (2c) of 5 μm up to a stress intensity of 5 $\text{MPa}\cdot\text{m}^{1/2}$ using crack growth constants (C and m) acquired from a power law fit of experimental data in this regime (FIB micro-notches). Small crack and long crack growth data appear to merge at stress intensities in the range of 5 $\text{MPa}\cdot\text{m}^{1/2}$, so beyond this point, the Paris law was integrated up to a crack size of 1 mm using crack growth constants extracted from a fit of the long crack growth portion of the (FSL generated) fatigue crack growth curves. The worst-case prediction was generated using the maximum observed small and long fatigue crack growth rates, while the less conservative of the two predictions uses the slowest small and long fatigue crack growth rates. Both sets of lifetimes were generated using a starting crack size of 5 μm and a final crack size of 1 mm. Thus, the bounds in fatigue crack growth behavior presented here result from the variability in measured fatigue crack growth rates and not from variability in the size of the fatigue crack initiation site. These crack growth-based predictions adequately capture the worst-case lifetimes to failure, however, they only account for approximately 0.1% of the variability observed in the total fatigue lifetimes of

unnotched round bar fatigue specimens. Thus, even when considering the variability in fatigue crack growth behavior at extreme value microstructural locations, the majority of scatter observed in fatigue lifetimes is still attributed to variability in fatigue crack initiation processes.

4. Conclusions

The variability in fatigue crack growth behavior resulting from differences in local texture was investigated with two $\alpha+\beta$ microstructures of Ti-6Al-2Sn-4Zr-6Mo; one containing microtexture (microstructure A) and another with a more random texture (microstructure B). In microstructure A, the local texture adjacent to the micro-notch was found to influence fatigue crack initiation lifetimes, with regions favorably oriented for basal and prism slip generally promoting early fatigue crack formation. However, growth rates did not correlate with local texture for individual cracks in either microstructure. The apparent absence of a local texture effect on fatigue crack growth rates may be attributed to a number of factors; the local textures investigated in this study may not be severe enough to influence growth rates, the two-dimensional characterization and classification of local microstructure may not provide sufficient detail to adequately describe local microstructural neighborhoods. Both of these limitations could be surmounted by testing material with higher degrees of microtexture and utilizing three-dimensional characterization tools.

Micro-notches with a surface length ($2c$) of approximately 20-25 μm exhibited sensitivity to local microstructure. For all notches of this size, approximately 1/2 of the notches were observed to initiate fatigue cracks. For notch lengths of 35 μm , these features were always observed to initiate fatigue cracks, indicating that they were larger than the size at which local

microstructure influences fatigue damage accumulation and propagation. Smaller notches, on the order of 15 μm , were never observed to initiate critical fatigue cracks. In specimens with notches of this size, cracks were observed to initiate elsewhere within the microstructure. This length scale is consistent with experimental measurements of crack initiation regions.

The fatigue crack growth rates measured using ultrasonic fatigue techniques are comparable to the fatigue crack growth rates measured at conventional frequencies of 20 Hz in both round bar fatigue specimens and in C(T) specimens. There is no difference in the initial small fatigue crack growth rates measured from naturally initiated fatigue cracks and those growth rates measured from FIB-machined micro-notches, which validates FIB-initiated crack growth rates as representative of the material microstructure. Both microstructural conditions exhibited a small crack effect, and growth rates merged with long crack growth rates at a stress intensity factor range of approximately $5 \text{ MPa}\cdot\text{m}^{1/2}$.

5. Acknowledgements

Financial support from AFOSR Metallic Materials Program (Project # F49620-03-1-0069) is gratefully acknowledged. One of the authors (CJS) would like to acknowledge funding from the STEP program at the AFRL Materials and Manufacturing Directorate.

Technical assistance from C. Torbet of the University of Michigan is appreciated. The experimental assistance of Mr. M. Eric Burba and Mr. Benjamin Briskin, both affiliated with AFRL, is also appreciated.

References

- [1] C.J. Szczepanski, S.K. Jha, J.M. Larsen, J.W. Jones. Microstructural Influences on Very-High-Cycle Fatigue-Crack Initiation in Ti-6246, *Metallurgical and Materials Transactions A*, 39A, (2008) 2841-2851.
- [2] C.J. Szczepanski. The role of microstructural variability on the very high cycle fatigue lifetime variability of the $\alpha + \beta$ titanium alloy, Ti-6Al-2Sn-4Zr-6Mo, Ph.D. Dissertation, University of Michigan, 2008.
- [3] J.A. Hall. Fatigue crack initiation in alpha-beta titanium alloys, *International Journal of Fatigue*, 31 (Suppl. 1), (1997) S23–S37.
- [4] G. Lutjering. Influence of processing on microstructure and mechanical properties of alpha + beta titanium alloys, *Materials Science and Engineering A*, A243 (1998) 32–45.
- [5] G. Luetjering and M. Peters. Mechanical Properties of a Titanium Blading Alloy, EPRI CS 2933. Project 1266-1. Final Report – Electric Power Research Institute - October 1983.
- [6] F. Larson, A. Zarkades. Properties of Textured Titanium Alloys, MCIC Report - MCIC-74-20 – Metals and Ceramics Information Center, June 1974.
- [7] S.K. Jha, M.J. Caton, J.M. Larsen. A new paradigm of fatigue variability behavior and implications for life prediction, *Materials Science and Engineering A*, A468-470 (2007) 23-32.
- [8] L. Christodoulou and J.M. Larsen. Using Materials Prognosis to Maximize the Utilization Potential of Complex Mechanical Systems, *Journal of Materials (JOM)*, March 2004, 15-19.
- [9] S.K. Jha, J.M. Larsen, A.H. Rosenberger, G.A. Hartman. Dual fatigue failure modes in Ti-6Al-2Sn-4Zr-6Mo and consequences on probabilistic life prediction, *Scripta Materialia* 48 (2003) 1637–1642.
- [10] D. L. Davidson, R. G. Tryon, M. Oja, R. Matthews, and K. S. Ravi Chandran. Fatigue crack initiation in Waspaloy at 20°C, *Metallurgical and Materials Transactions A*, 38 (2007) 2214–2225.
- [11] V. Sinha, J. E. Spowart, M. J. Mills, and J. C. Williams. Observations on the faceted initiation site in the dwell-fatigue tested Ti-6242 alloy: Crystallographic orientation and size effects, *Metallurgical and Materials Transactions A*, 37A (2006) 1507-1518.
- [12] K. LeBiavant, S. Pommier, and C. Prioul. Local texture and fatigue crack initiation in a Ti-6Al-4V titanium alloy, *Fatigue and Fracture of Engineering Materials and Structures*, 25 (2002) 527–545.
- [13] F. Bridier, P. Villechaise, J. Mendez. Slip and fatigue crack formation processes in an α/β titanium alloy in relation to crystallographic texture on different scales, *Acta Materialia* 56 (2008) 3951–3962.

- [14] I. Bantounas, D. Dye, T.C. Lindley. The effect of grain orientation on fracture morphology during high-cycle fatigue of Ti-6Al-4V. *Acta Materialia* 57 (2009) 3584–3595.
- [15] M. Brogdon and A.H. Rosenberger. Evaluation of the influence of grain structure on the fatigue variability of Waspaloy, *Superalloys 2008*, 583-588.
- [16] S.K. Jha and J.M. Larsen. Random heterogeneity scales and probabilistic description of the long-lifetime regime, in *VHCF4*, J. Allison, J.W. Jones, J. Larsen, and R. Ritchie, eds., TMS, Warrendale, PA, 2007, 385–96.
- [17] M. Peters, A. Gysler, G. Lutjering. Influence of Texture on Fatigue Properties of Ti-6Al-4V, *Metallurgical Transactions* 15A (1984) 1597-1605.
- [18] A.W. Bowen. The influence of crystallographic orientation on fatigue crack growth in strongly textured Ti-6Al-4V. *Acta Metallurgica*, 23 (1975) 1401–1409.
- [19] A. P. Woodfield, M. D. Gorman, R. R. Corderman, J. A. Sutliff, and B. Yamrom. Effect of microstructure on dwell fatigue behavior of Ti-6242. In *Titanium '95*. Vol. II, Institute of Materials, Birmingham, UK, 1996, 1116–1123.
- [20] I. Bantounas, T.C. Lindley, D. Rugg, and D. Dye. Effect of microtexture on fatigue cracking in Ti-6Al-4V, *Acta Materialia*, 55 (2007) 5655–5665.
- [21] T. Zhai, A.J. Wilkinson, J.W. Martin. Crystallographic Mechanism for Fatigue Crack Propagation through Boundaries, *Acta Materialia*, 48 (2000) 4917–4927A.
- [22] T. Zhai. The effects of macro- and micro-texture on the fatigue properties of Al-Li 8090 alloys, *Proceedings from Materials Solutions Conference*, Indianapolis, IN, ASM International, 5-8 November 2001, 83-91.
- [23] M. Marx, W. Schaef, H. Vehoff. Interaction of short cracks with the local microstructure, *Fatigue 2010, Procedia Engineering*, 2 (2010) 163-171.
- [24] U. Krupp, W. Floer, J. Lei, Y. Hu, H. Christ, A. Schick, C. Fritzen. Mechanisms of short-fatigue-crack initiation and propagation in a β -Ti alloy, *Philosophical Magazine A*, 82 (2002) 3321-3332.
- [25] Y. Saleh, H. Margolin, Low cycle fatigue of Ti-Mn alloys: microstructural aspects of fatigue crack growth, *Metallurgical Transactions*, 14A (1983) 1481-1486.
- [26] E.B. Shell, S.L. Semiatin. Effect of initial microstructure on plastic flow and dynamic globularization during hot working in Ti-6Al-4V, *Metallurgical and Materials Transactions*, 30A, December 1999, 3219-3229.
- [27] T.R. Bieler, and S.L. Semiatin. The origins of heterogeneous deformation during primary hot working of Ti-6Al-4V, *International Journal of Plasticity (UK)*, 18 (2002) 1165-1189

- [28] J. M. Larsen, J. R. Jira, and K. S. Ravichandran. Measurement of small cracks by photomicroscopy: Experiments and analysis. In STP 1149, ASTM, Philadelphia, PA, 1992. 57–80.
- [29] Q. Feng, Y. Picard, H. Liu, S. Yalisove, G. Mourou, and T. M. Pollock. Femtosecond laser micromachining of a single-crystal superalloy. *Scripta Materialia*, 53:511–516, 2005.
- [30] A. Shyam, C. Torbet, S. K. Jha, J. Larsen, M. Caton, C. Szczepanski, T. M. Pollock, and J. W. Jones. Development of ultrasonic fatigue for rapid, high temperature fatigue studies in turbine engines, In *Superalloys 2004*, K. Green, T. M. Pollock, H. Harada, T. Howson, R. Reed, J. Schirra, and S. Walston, eds., TMS (2004) 259–268.
- [31] X. Zhu. Ultrasonic fatigue of E319 cast aluminum alloy in the long lifetime regime, PhD thesis, University of Michigan, 2007.
- [32] J. Orloff, M. Utlaut, L. Swanson. *High Resolution Focused Ion Beams: FIB and its applications*, Kluwer Academic/Plenum Publishers. 2003.
- [33] J.C. Williams, R.G. Baggerly, and N.E. Paton. Deformation behavior of HCP Ti-Al alloy single crystals, *Metallurgical and Materials Transactions*, 33A (2002) 2015–2026.
- [34] J. Newman and I. Raju. An empirical stress-intensity factor equation for the surface crack, *Engineering Fracture Mechanics*, 15 (1981) 185–192.
- [35] K.S. Chan and J. Lankford. The role of microstructural dissimilitude in fatigue and fracture of small cracks, *Acta Metallurgica*, 36 (1988) 193–206.
- [36] S. Suresh and R.O. Ritchie. Propagation of short fatigue cracks, *International Materials Reviews*, 29 (1984) 445-476.
- [37] C.J. Szczepanski, A. Shyam, S.K. Jha, J.M. Larsen, C.J. Torbet, S.J. Johnson, J.W. Jones. Characterization of the role of microstructure on the fatigue life of Ti-6Al-2Sn-4Zr-6Mo using ultrasonic fatigue, in *Materials Damage Prognosis*, Eds. J.M. Larsen, L. Christodoulou, J.R. Calcaterra, M.L. Dent, M.M. Deriso, W.J. Hardman, J.W. Jones and S.M. Russ. TMS 2005, 315-320.
- [38] J.M. Larsen, unpublished research, 1992.

Figure Captions

Figure 1 – (a) Backscattered electron (BSE) micrograph of microstructure A, (b) BSE micrograph of microstructure B, (c) Inverse Pole Figure (IPF) map of the β phase from microstructure A, (d) IPF map of the β phase from microstructure B.

Figure 2 – (a) Schematic of specimen with flats and multiple micro-notches. The specimen gage is 12 mm long and 4 mm in diameter. After machining the flats, the specimen thickness in the gage is approximately 3.2 mm. The distance between micro-notches is 2-3 mm. (b) Representative notch produced with a focused ion beam (FIB) microscope (2c~14 μm).

Figure 3 – α phase IPF map, β phase IPF map, and IPFs calculated along loading axis corresponding to the first four cracks to form in specimen from microstructure A. Neighborhoods shown here correspond to crack IDs in Figure 13(a) and (b) as follows: (a) A7, (b) A8, (c) A6, (d) A3.

Figure 4 – α phase IPF map, β phase IPF map, and IPFs calculated along loading axis corresponding to the second four cracks to form in specimen from microstructure A. Neighborhoods shown here correspond to crack IDs in Figure 13(a) and (b) as follows: (a) A2, (b) A5, (c) A4, (d) A1.

Figure 5 – α phase IPF map, β phase IPF map, and IPFs calculated along loading axis corresponding to the first four cracks to form in specimen from microstructure B. Neighborhoods shown here correspond to crack IDs in Figure 13(c) and (d) as follows: (a) B3, (b) B1, (c) B7, (d) B4.

Figure 6 – α phase IPF map, β phase IPF map, and IPFs calculated along loading axis corresponding to the second four cracks to form in specimen from microstructure B. Neighborhoods shown here correspond to crack IDs in Figure 13(c) and (d) as follows: (a) B5, (b) B2, (c) B8, (d) B6.

Figure 7 –Legends for IPF maps illustrating the (a) α phase orientations, (b) β phase orientations, and (c) the locus of Schmid factor maxima ($SF \geq 0.475$) for basal, pyramidal, and prism slip.

Figure 8 – da/dN plots illustrating small fatigue crack growth rates for conventional and ultrasonic frequencies, along with predictions generated from long crack growth rates.[27,38] Conventional frequency data from [7].

Figure 9 - Plot of the fraction of notches initiating fatigue cracks as a function of the notch size. It should be noted that one specimen from microstructure B with an 18 μm notch failed from a subsurface crack initiation site.

Figure 10 – (a) A BSE micrograph of a 15 μm notch in a specimen from microstructure B that initiated a fatigue crack, but did not lead to failure. (b) Fractograph illustrating the facet at the subsurface fatigue crack initiation site.

Figure 11 – Fatigue crack growth rates for microstructure A (gray solid triangles) and microstructure B (black open circles) measured at 20 kHz, R=0.05, room temperature, and $\sigma_{\text{max}}=600$ MPa. The solid line is a long crack growth rate prediction for the same alloy.[27]

Figure 12 – (a) $2c$ vs. N plot and (b) fatigue crack growth rate plot for specimen from microstructure A. (c) $2c$ vs. N plot and (d) fatigue crack growth rate plot for specimen from microstructure B. All cracks were tested at 20 kHz, R=0.05, room temperature, and $\sigma_{\text{max}}=600$ MPa.

Figure 13 – This plot illustrates the texture intensity and the most favorable slip system within each microstructural neighborhood surrounding the notches in (a) microstructure A and (b) microstructure B.

Figure 14 – (a) BSE micrograph of the fastest growing crack (crack A6) in microstructure A and (b) the crack (crack A8) with the slowest propagation rate in microstructure A, both of which are annotated with cycle count and crack length as measured from acetate replicas.

Figure 15 – (a) and (b) are Schmid factor maps in the neighborhood surrounding the fastest growing crack (A6) in microstructure A, for basal and prism slip, respectively. (c) and (d) are the same Schmid factor plots for the slowest growing crack in the same specimen (A8). The white traces indicate the location of the FIB micronotch and the subsequent crack path.

Figure 16 – Fatigue lifetime data of Ti-6246 with predictions of the worst case lifetime as determined by integration of the small and long fatigue crack growth data from a starting crack size of $a=5$ μm up to a final crack size of 1 mm.

Table I. The cycle count and relative rankings of fatigue crack growth rates measured from the cracks shown in Figure 3 and 4.

Table II. The cycle count and relative rankings of fatigue crack growth rates measured from the cracks shown in Figure 5 and 6.

Figures

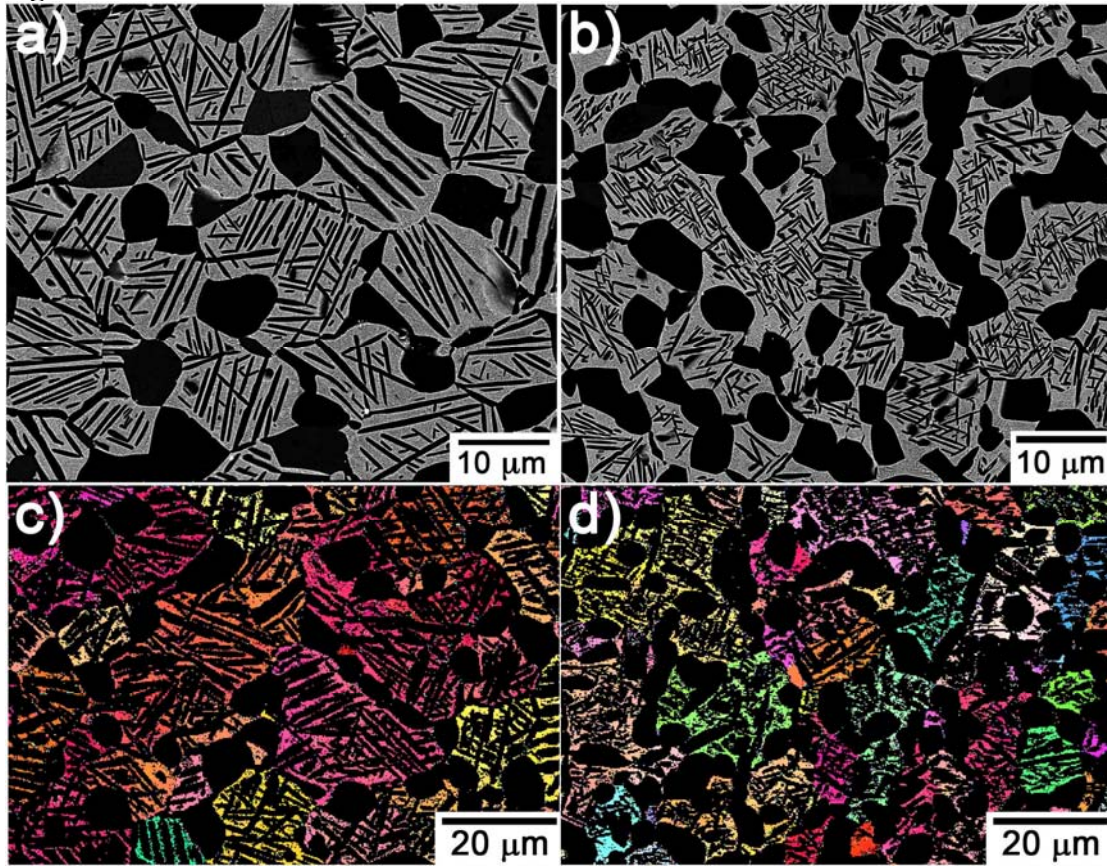


Figure 1.

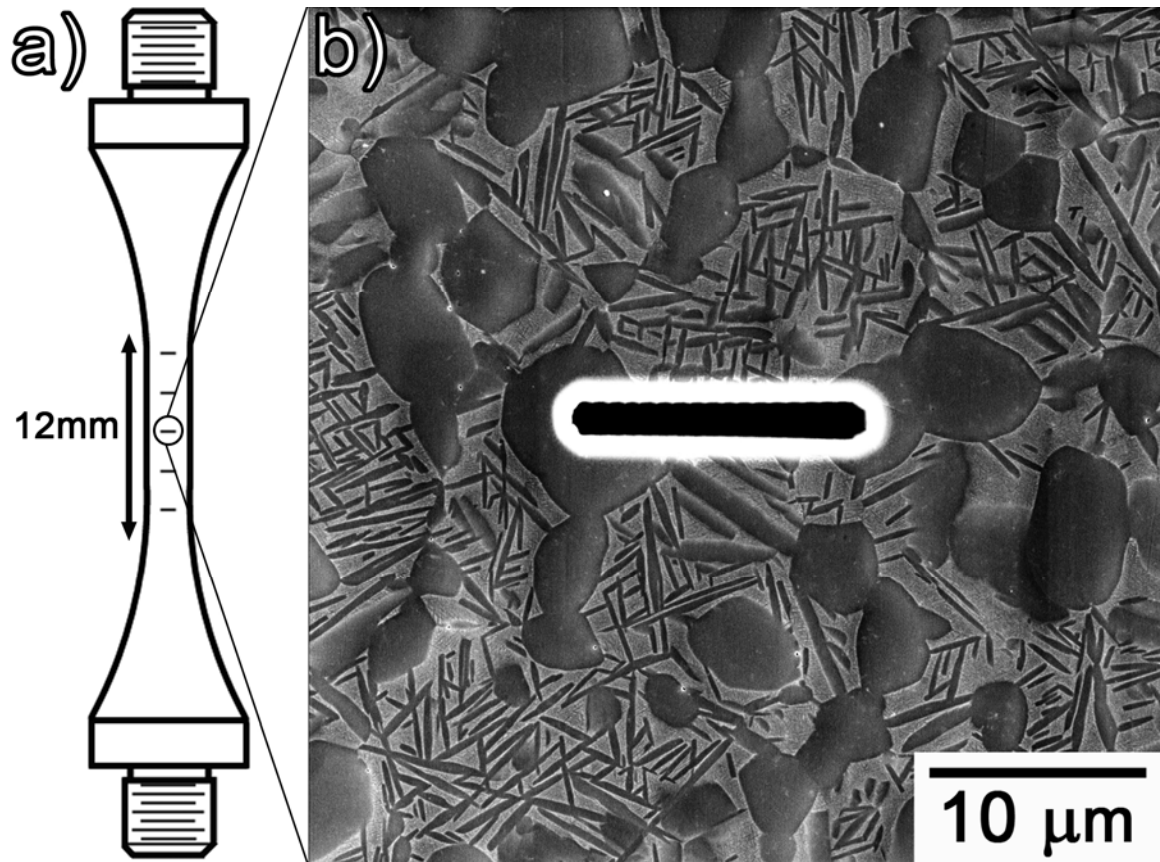


Figure 2

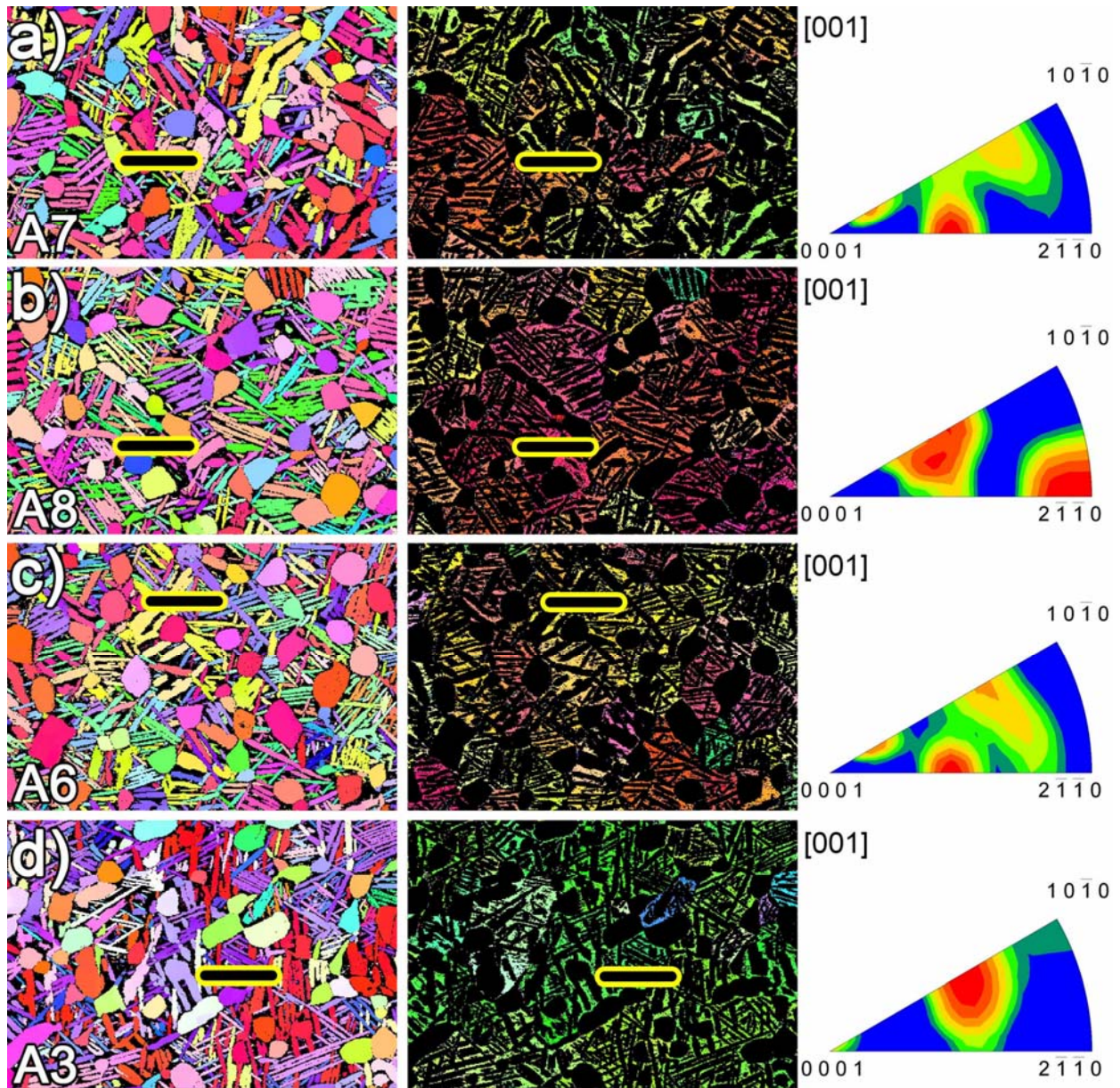


Figure 3.

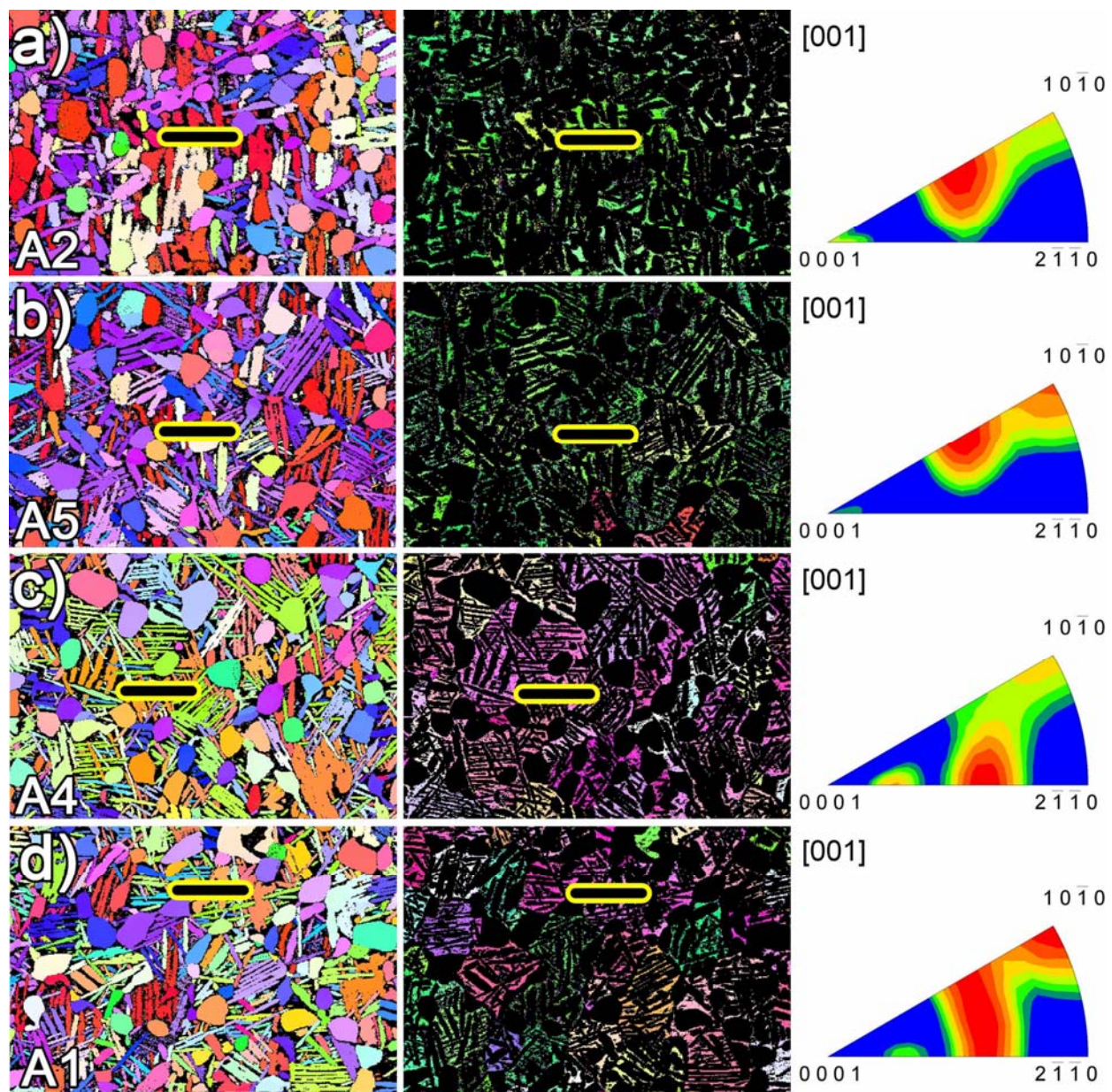


Figure 4.

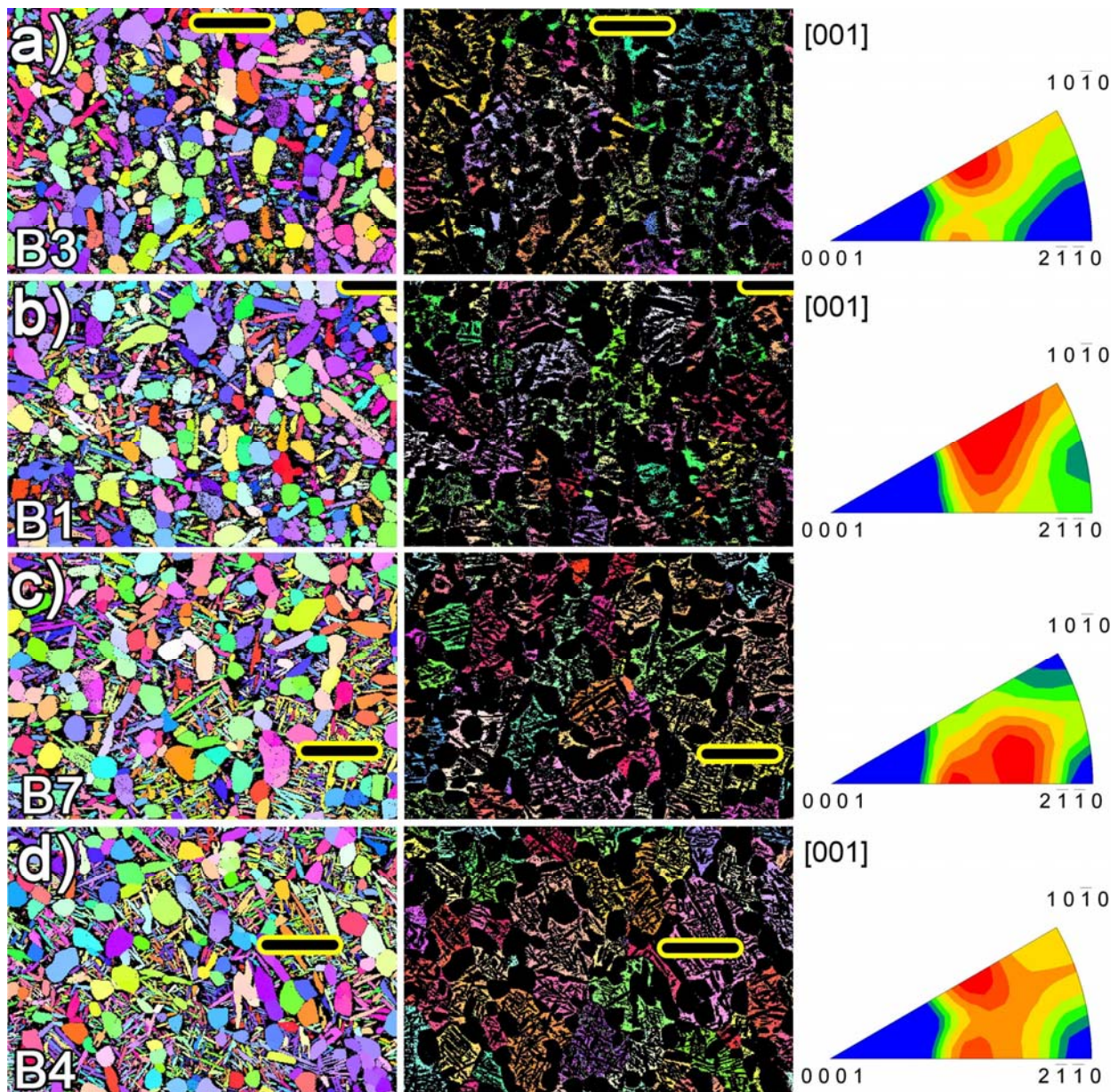


Figure 5.

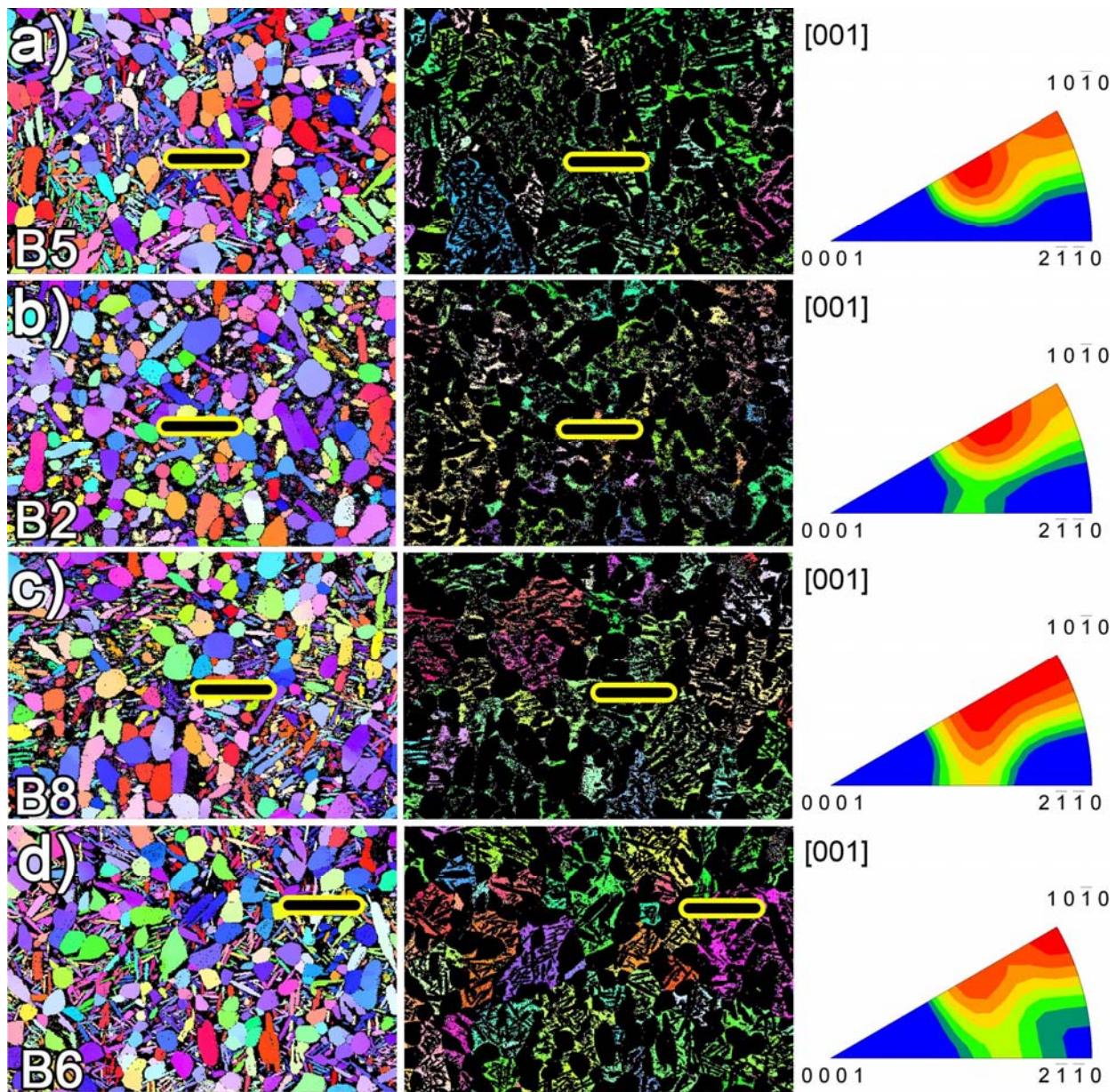


Figure 6.

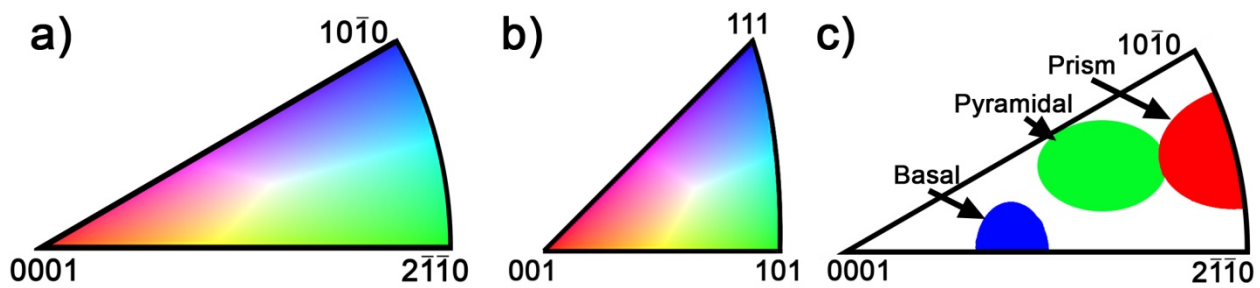


Figure 7.

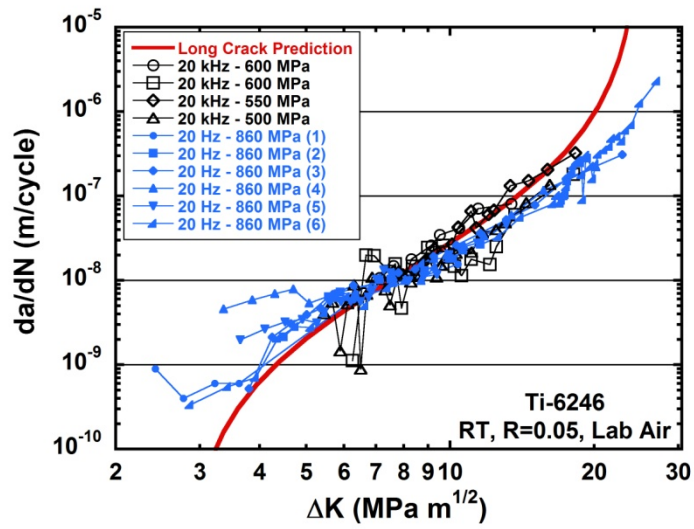


Figure 8.

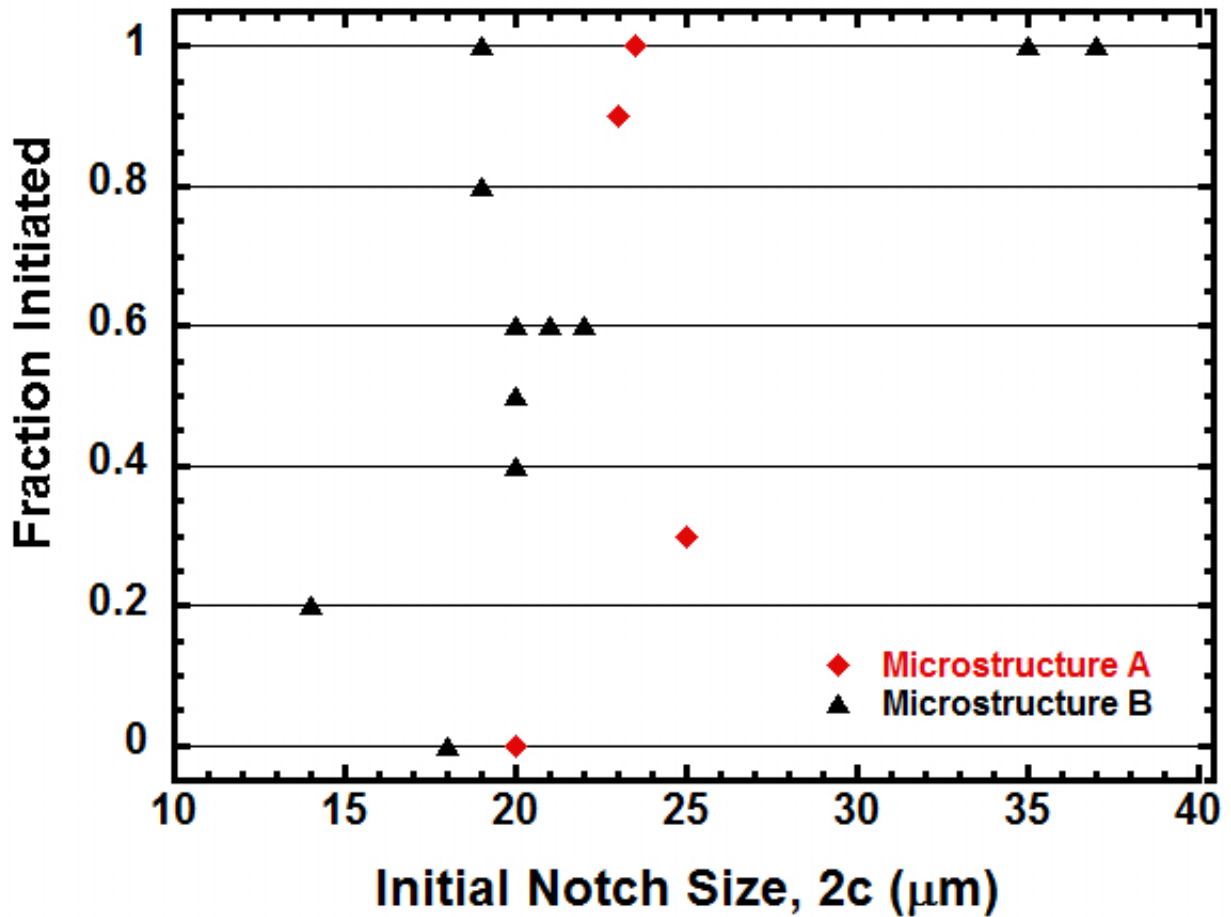


Figure 9.

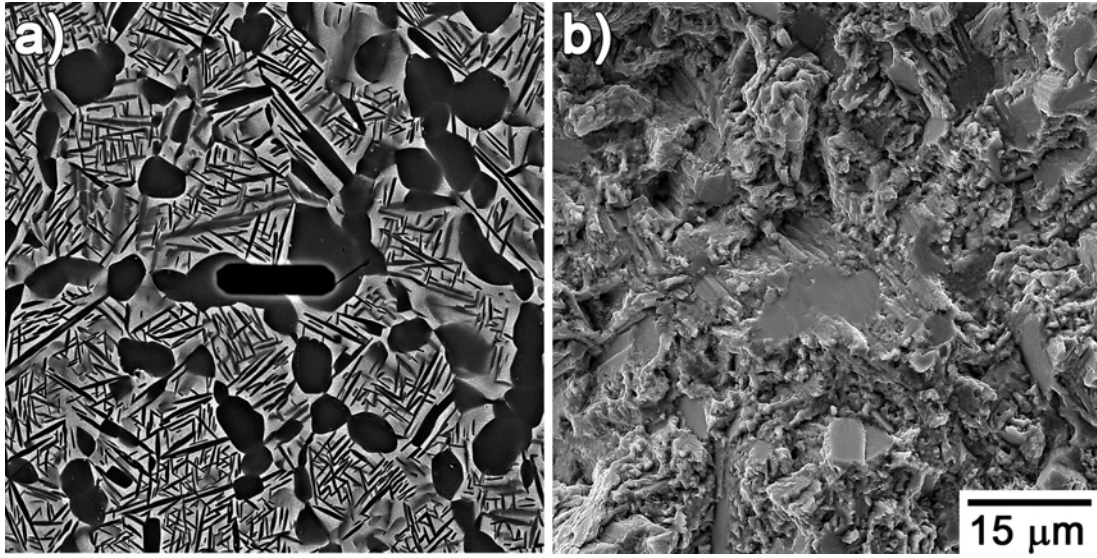


Figure 10.

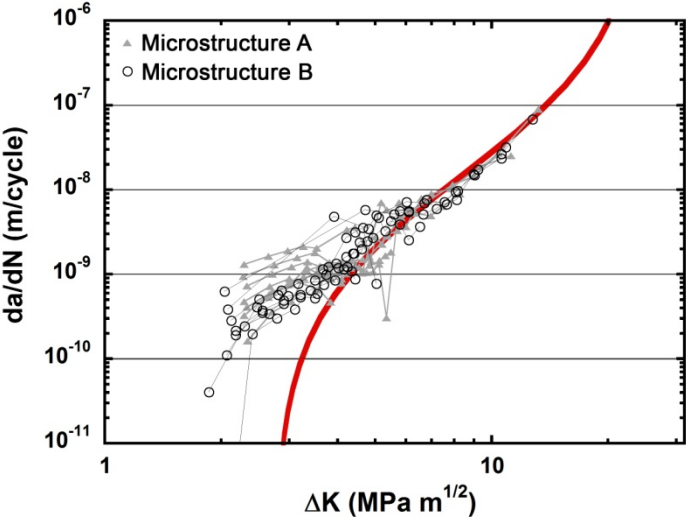


Figure 11.

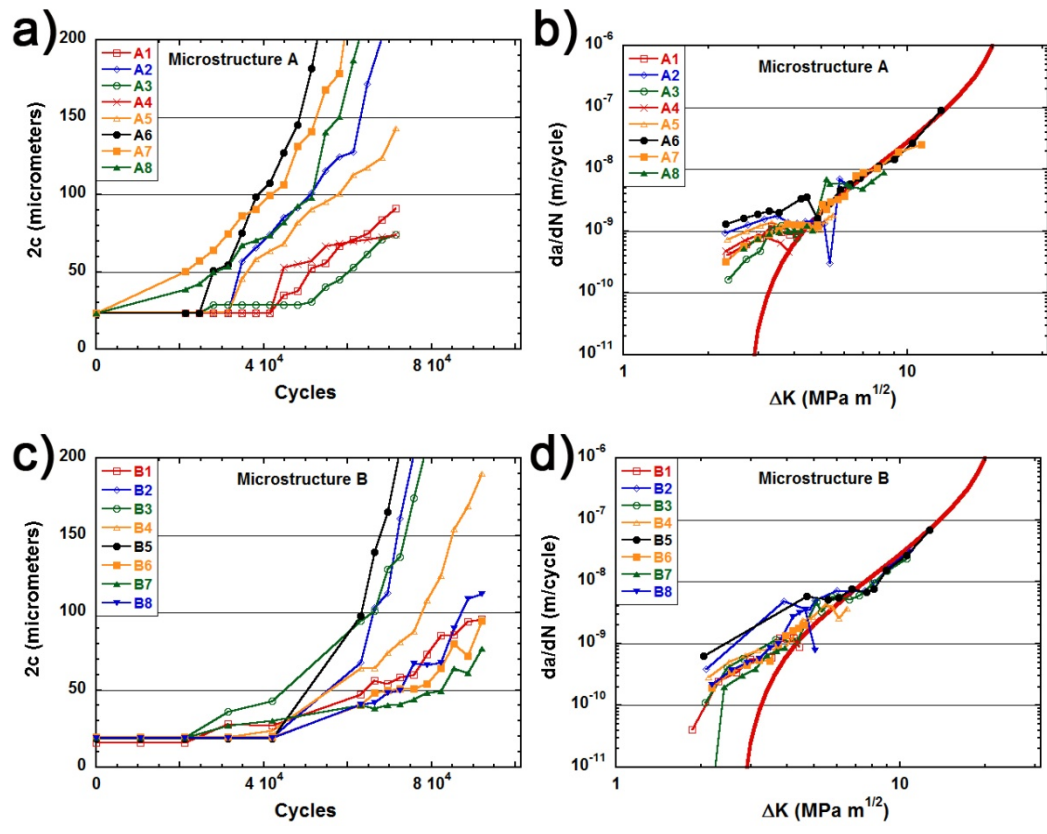


Figure 12.

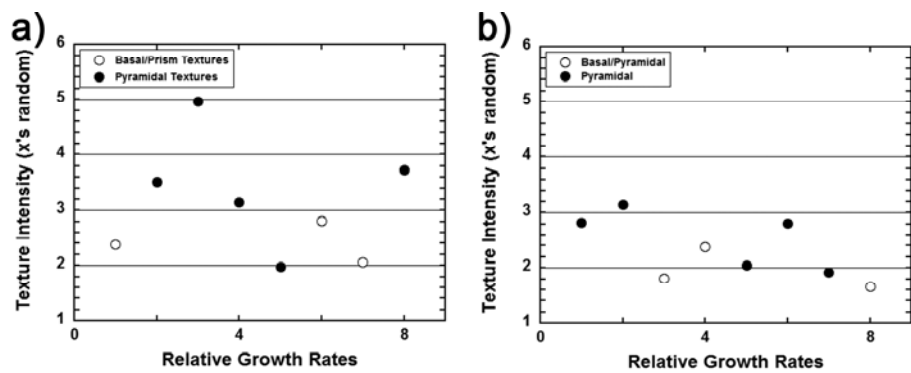


Figure 13.

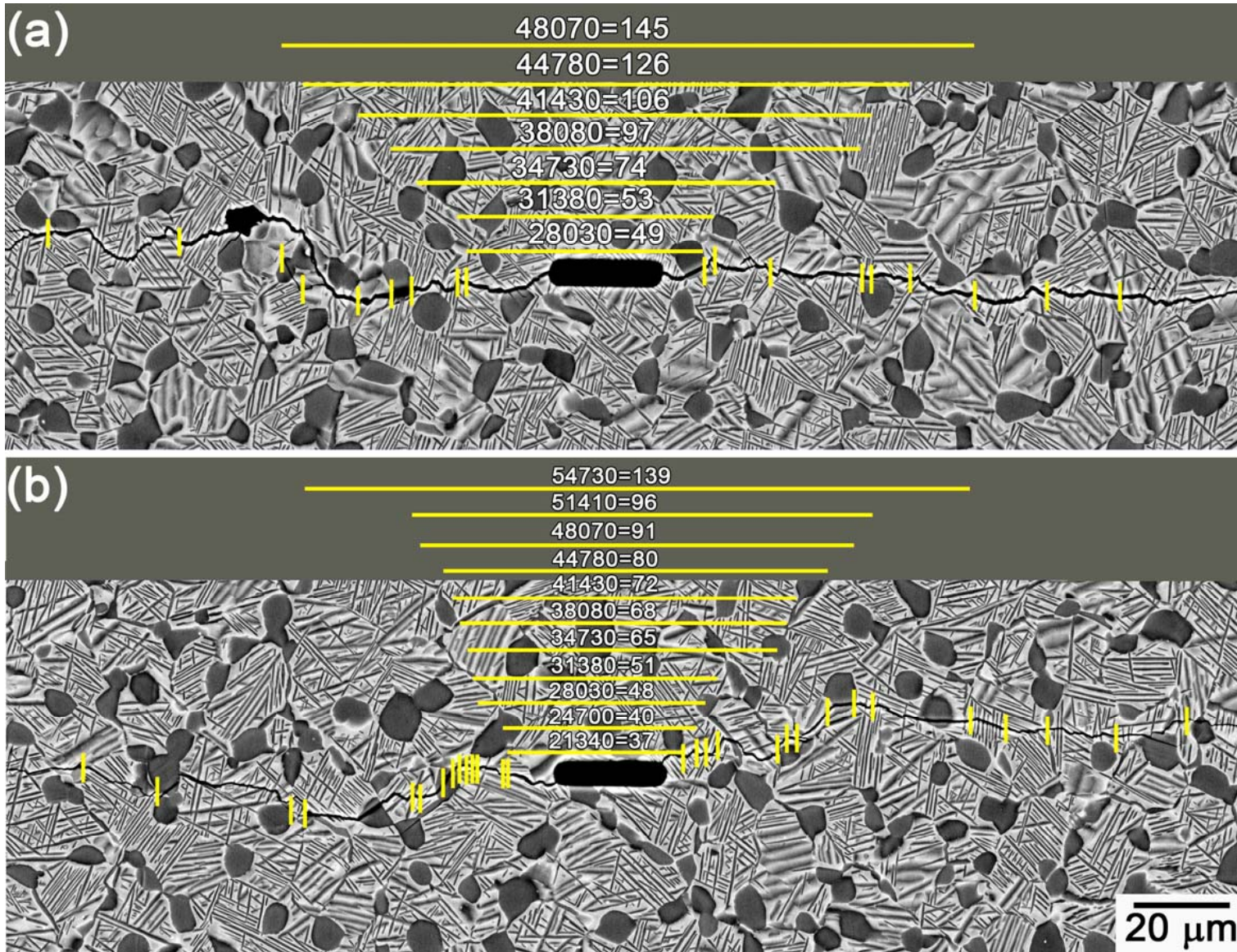


Figure 14.

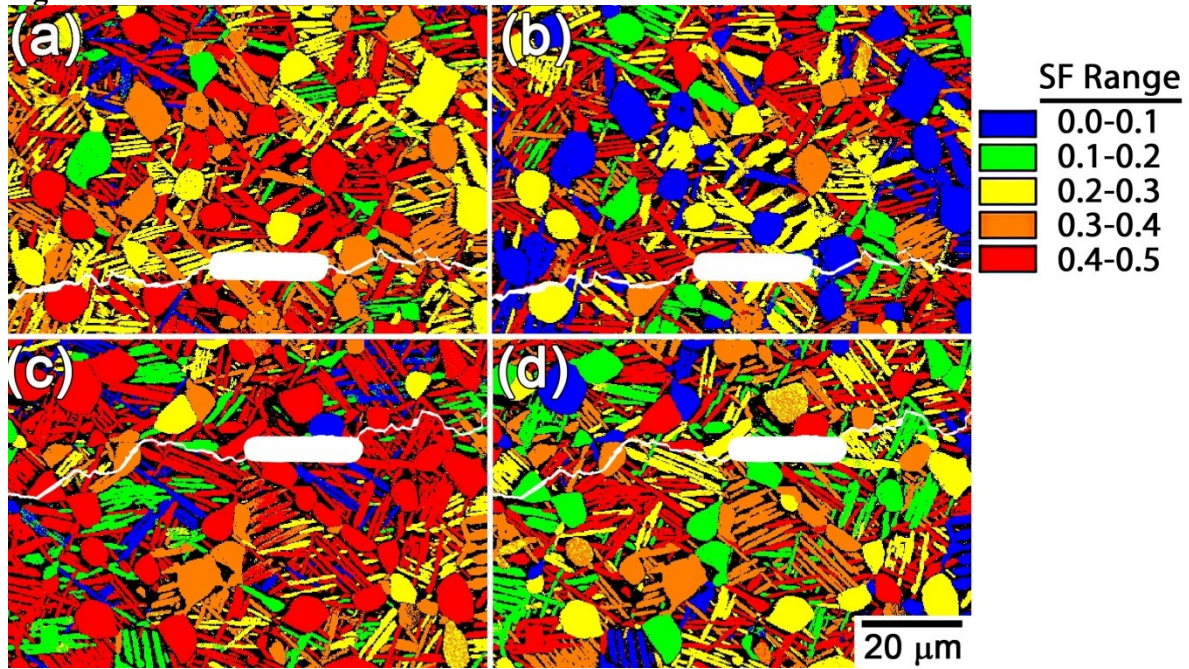


Figure 15.

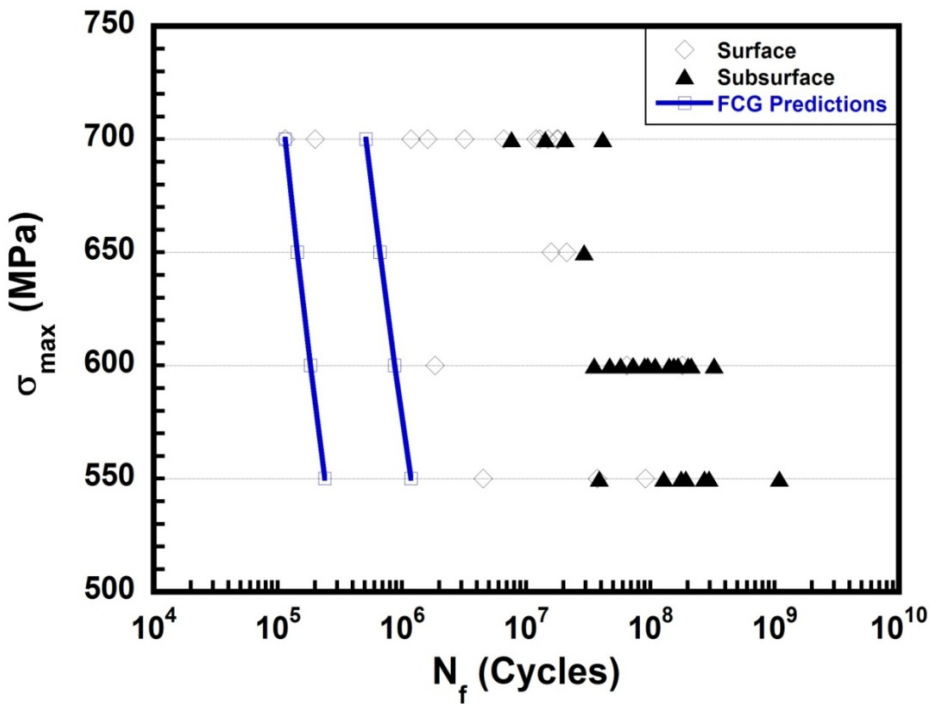


Figure 16.

Table I.

Crack ID	Initiation Lifetime (cycles)	Relative Propagation Rates	Figure
A7	21340	6	3(a)
A8	21340	7	3(b)
A6	28030	1	3(c)
A3	28030	8	3(d)
A2	34730	2	4(a)
A5	34730	3	4(b)
A4	44780	4	4(c)
A1	44780	5	4(d)

Table II.

Crack ID	Initiation Lifetime (cycles)	Relative Propagation Rates	Figure
B3	31370	4	5(a)
B1	31370	7	5(b)
B7	31370	8	5(c)
B4	41950	3	5(d)
B5	63120	1	6(a)
B2	63120	2	6(b)
B8	63120	5	6(c)
B6	63120	6	6(d)